PHYSICAL REVIEW B **79**, 020202(R) (2009)

Martensitic transformation path of NiTi

N. Hatcher,[1] O. Yu. Kontsevoi,[1] and A. J. Freeman[1,2]
[1]*Department of Physics and Astronomy, Northwestern University, Evanston, Illinois 60208, USA*
[2]*Department of Materials Science and Engineering, Northwestern University, Evanston, Illinois 60208, USA*
(Received 11 November 2008; published 13 January 2009)

We present the structural evolution mechanism during the NiTi martensitic transformation and show the origins of this behavior in electronic and phononic anomalies. By employing highly precise all-electron density-functional theory calculations, we establish a barrierless transformation path for equiatomic NiTi consisting of a basal shear composed of bilayer ⟨100⟩{011} stacking faults to the B2 phase followed by another basal shear which causes a relaxation of the structure's monoclinic angle and results in the B19′ phase. This path is traced to evolving Fermi-surface nesting regions, which drive the structural transformation between the austenitic and martensitic phases.

DOI: 10.1103/PhysRevB.79.020202 PACS number(s): 64.70.kd, 71.20.Be

The importance of thermomechanical and piezomechanical engineering and design has generated considerable interest in equiatomic NiTi (nitinol) for its exhibition of a reversible martensitic transformation near room temperature and shape memory effect. With an abundance of possible applications as medical devices and materials for aerospace, industrial, and commercial use, a full understanding of why and how this crystal undergoes a structural transformation is crucial. However, despite great progress toward understanding this material both theoretically and experimentally, the atomistic model for this transformation path is not well established. Here we present a mechanism for this transformation and uncover the underlying cause of its behavior.

In total, there are four different phases that have been observed throughout the martensitic transformation of NiTi: B2, R, B19, and B19′. The high-temperature austenite B2 phase transforms to the low-temperature martensite B19′ phase upon cooling either directly or through intermediate B19 or R phases if alloyed with ternary elements such as Cu and Fe, respectively. Here we seek an understanding of the direct equiatomic NiTi transformation path from B2 to B19′, which is still not clearly established. Otsuka and Ren[1] proposed that this transformation occurs by the application of a $\langle 1\bar{1}0\rangle\{110\}$ basal shear/shuffle followed by a $\langle 1\bar{1}0\rangle\{001\}$ nonbasal shear and that, in the absence of the nonbasal shear, NiTi evolves to the B19 structure similar to that of many other Ti alloys (e.g., TiPd, TiNiPd, and TiAu). More recently, Huang *et al.*[2] proposed that the martensitic phase was not the B19′ structure that was established by experiment and previous calculations[3–8] but rather a base-centered-orthorhombic (BCO) structure and that B19′ is instead effectively stabilized by internal stresses. Subsequently, Morris *et al.*[9] calculated a transformation from B2 to this BCO phase, which they identified as B33. The transformation involves shuffling pairs of {011} planes via stacking faults which leads to the orthorhombic B33 structure. To date there is no established atomistic transformation path. In this Rapid Communication we resolve these issues by first investigating those previously proposed paths and then clearly establish a direct transformation path for NiTi.

To fully understand the structural evolution of the phases, we first calculated their total energies and structural parameters (see Table I). All calculations were performed using the highly precise full-potential linearized augmented plane-wave (FLAPW) method.[13] The exchange-correlation contribution to the potential was included using the generalized gradient approximation within the Perdew-Burke-Ernzerhof functional.[14] The plane-wave cutoff was set to 218 eV and the cutoff of the potential representation was set to 1360 eV. The mesh of up to 33 000 k points in the irreducible Brillouin zone was chosen to ensure a total-energy convergence within 0.4 meV/atom. The muffin-tin radii of Ti and Ni atoms were taken to be 2.35 and 2.10 a.u., respectively. For a more accurate treatment of extended core electrons (i.e., Ti 3p electrons), the method of explicit orthogonalization was used.[15] Structural optimization was performed for each structure for all lattice constants, angles, and internal atomic coordinates.

Our results agree well with the precisely measured lattice constants, crystal structures, and formation energies for each of the different phases [for example, we calculated a B2 formation energy of 34.2 kJ/(mol atom) versus a measured value of 33.9 kJ/(mol atom)].[16] The calculated total energies are consistent with experimental findings: the high-temperature austenitic B2 phase has the highest relative total energy, B19′ has the lowest, and each intermediate structure's energy lies between these extrema.

Experiments and calculations have established that the B2 phase, which is only stable at high temperatures, exhibits precursory behavior toward a structural transformation due to softening of the TA_2 phonon modes[17,18] and small elastic constants. We calculated all independent elastic constants for each phase. The C_{44} and C' elastic constants were 46 and 19 GPa, respectively, for the B2 phase and 87 and 60 GPa for the B19′ phase. The low values of the austenitic phase compared to the martensitic phase indicate that the B2 phase is unstable to deformation which may be exhibited as the temperature is decreased.

Since the initial characterization of the phases of martensitic NiTi, researchers have assumed that there is a direct transformation path between the B2 and the B19′ phases that may be inferred from these precursory phenomena in the B2 phase. Otsuka and Ren[1] tied the soft C', C_{44}, and TA_2 phonon modes to $\langle 1\bar{1}0\rangle\{110\}$ basal shear/shuffle and $\langle 1\bar{1}0\rangle\{001\}$ nonbasal shear instabilities, which comprise the atomistic transformation path. We performed calculations involving

TABLE I. Calculated structural parameters and total energies relative to the B2 structure among the different optimized structures of NiTi. Lattice-constant lengths a, b, and c are given in Å; nonright angles are stated. Volume is given in $Å^3/z$ where z is the number of f.u./unit cell.

Structure	Space group	z	a	b	c	Angle	Volume	$E-E_{B2}$ (meV/atom)
				Results of this work				
B2	$Pm\bar{3}m$	1	3.019				27.516	0.0
R	$P3$	9	7.301		5.353	$\gamma=120°$	27.452	−33.9
B19	$Pcmm$	2	4.615	4.152	2.851		27.319	−40.6
109°-B19′	$P2_1/m$	2	4.707	4.159	2.933	$\beta=108.88°$	27.281	−25.2
B19′	$P2_1/m$	2	4.674	4.085	2.919	$\beta=99.09°$	27.517	−57.2
				Experiments/previous calculations				
B2[a]	$Pm\bar{3}m$	1	3.013				27.339	
R[b]	$P3$	9	7.358		5.286	$\gamma=120°$	27.533	
B19[c]	$Pcmm$	2	4.510	4.224	2.899		27.614	
B33[d]	$Cmcm$	2	5.072	4.076	3.300	$\beta=108°$	32.442	
B19′ [e]	$P2_1/m$	2	4.66	4.11	2.91	$\beta=98°$	27.596	

[a]Experimental results by Sittner *et al.* (Ref. 10).
[b]Experimental results by Hara *et al.* (Ref. 11).
[c]Experimental results by Nam *et al.* (Ref. 12).
[d]Calculated results by Morris *et al.* (Ref. 9).
[e]Experimental results by Prokoshkin *et al.* (Ref. 8).

this basal shear and discovered that there is excessive Ti-Ti repulsion which cannot be accommodated by atomic relaxation. Thus, this transformation cannot be made without an energy barrier. We further performed calculations for an alternative path involving a single-layer ⟨100⟩{011} basal shear and also found excessively high-energy barriers due to Ti-Ni repulsive forces. These findings show that monolayer shears are improbable.

In order to devise another transformation path, we calculated generalized stacking fault energies, also referred to as γ surfaces,[19] for low-index shear planes. These γ surfaces for the B2 phase, calculated using a rigid shift of a supercell along the {001} and {011} slip planes with six atomic layers, revealed a prohibitively high-energy barrier to shear in all directions for {001} slip. However, the {011} slip barriers were much lower; in the ⟨111⟩ direction, the barrier was 0.890 J/m^2 (see Fig. 1). Using full relaxation, we found that the low-energy barrier path decreased drastically to 0.108 J/m^2 and changed from the ⟨110⟩ direction to the ⟨100⟩ direction. This was facilitated by significant movement of the atomic coordinates: the Ti-Ni bonds equalize, lowering their interatomic repulsion and reducing the resistance to ⟨100⟩{011} shear.

A reduction in the number of shear layers from six reduced the ⟨100⟩{011} energy barrier further. Setting the number of {011} planes to two and alternating shear direction

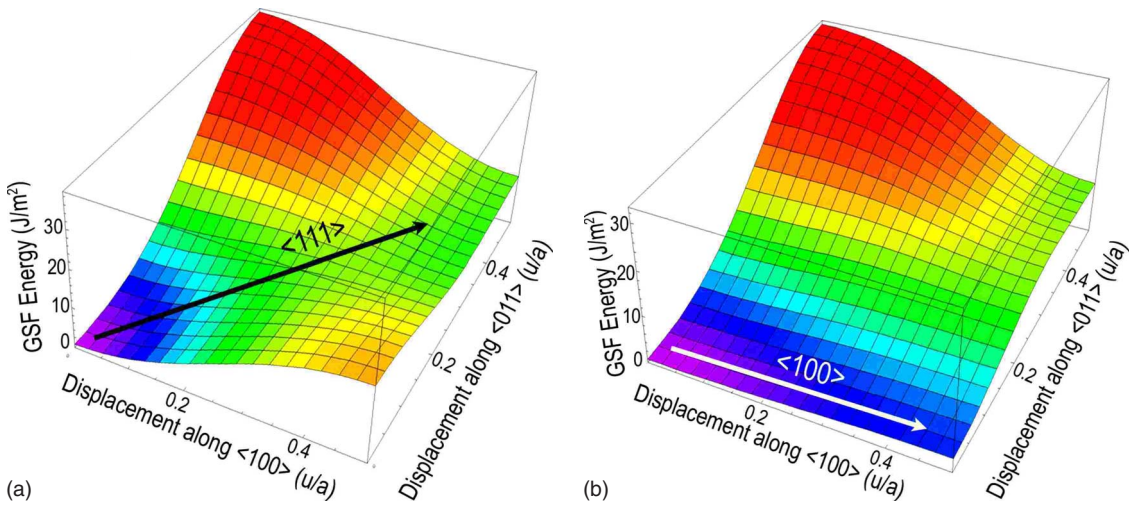

FIG. 1. (Color online) The γ surface for the {011} slip plane. For (a), no relaxation was employed. For (b), lattice parameters and atomic coordinates were relaxed.

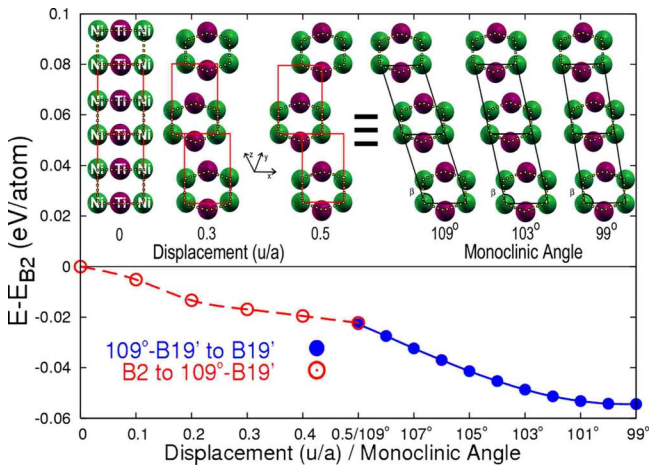

FIG. 2. (Color online) Top: the relaxed NiTi transformation is viewed along the {011} plane from B2 to 109°-B19′ where solid lines outline the unit cell and dotted lines mark the bilayers. The coordinate system is relative to the B2 phase. Bottom: total energies relative to the initial B2 phase are plotted against a relative shear along the slip plane for the B2 phase to the 109°-B19′ path and changes to the monoclinic angle for the 109°-B19′-B19′ phase path.

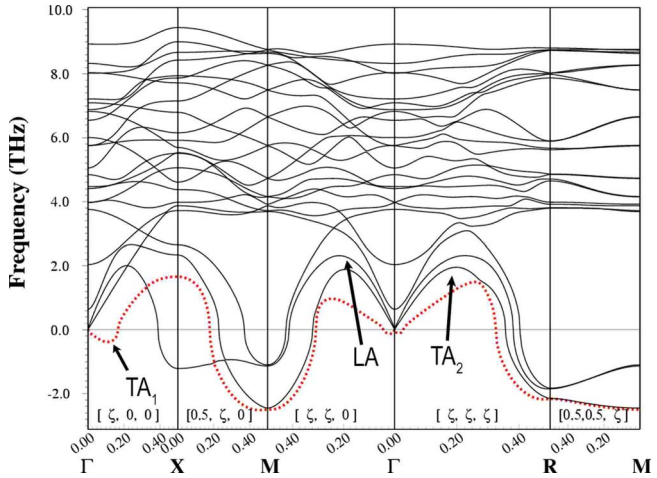

FIG. 3. (Color online) The phonon spectrum of NiTi at 0.2 ⟨100⟩{011} bilayer shear from the B2 structure calculated using the direct method (Ref. 24). While initially the instability in the phonon spectrum to the B2 structure lies in the TA_2 and LA modes in the ⟨110⟩ and ⟨111⟩ directions (Ref. 18), the application of a 0.2 ⟨100⟩{011} bilayer shear dramatically changes the phonon spectrum by lowering the TA_1 mode (dashed line) below the others.

("shuffle") created the unique result of a barrierless path in the ⟨100⟩ direction (similar behavior was observed by Morris *et al.*[9] for NiTi and CoZr). The transformation is illustrated in Fig. 2 such that the {011} plane is perpendicular to the vertical axis at each displacement step, and the stacking fault between each pair of planes is induced in the ⟨100⟩ direction. We calculated the total energy, crystal structure, and atomic positions at each $0.1a$ step until a displacement of $0.5u/a$ is reached and plotted the total energy of the NiTi transformation path below. At each point a full optimization is performed to obtain the lowest-energy state of each step. The structural evolution of this transformation is as follows. The initial B2 phase, $Pm\bar{3}m$ space group, is represented by a zero relative shift. The bilayer ⟨100⟩{011} basal shear/shuffle breaks cubic symmetry and it becomes orthorhombic with space group *Pcam*. When the shear reaches $0.5u/a$ displacement, the primitive unit cell becomes equivalent to the monoclinic-type B19′ and its monoclinic angle β is 109°. We will call this point 109°-B19′. The transformation path is continuous and barrierless to 109°-B19′, which has a total energy of 25.2 meV/atom lower than B2.

Since B19′ has a lower total energy than 109°-B19′, there must be a transformation path between the two structures. Upon comparison, we determined the primary difference between these two structures was their monoclinic angles β. We relaxed the β angle of 109°-B19′, effectively inducing a ⟨100⟩{011} basal shear (see Fig. 2). When β =99°, the structure becomes B19′. This angle relaxation is the second barrierless step of the transformation. Thus, we have established that the only possible direct continuous barrierless transformation from the B2 phase to the B19′ phase is this two-step transformation consisting of a ⟨100⟩{011} bilayer basal shear/shuffle followed by another basal shear which causes a relaxation of the structure's monoclinic angle and results in the B19′ phase with a minimum total energy that is 57.2 meV/atom below B2.

Now, a recent development in the understanding of the structural transformation of NiTi is a suggestion by Huang *et al.*[2] and Morris *et al.*[9] that the martensitic phase of NiTi is BCO (labeled B33 by Morris *et al.*) rather than B19′. We first repeated these calculations using the structural parameters provided by Huang *et al.* and determined the total energy of BCO to be 3 meV/atom lower than the B19′ phase. While lower, this energy difference is very small (~35 K), and further study concerning its relation to the B2 structure is warranted. Additionally, the primitive unit cell is monoclinic, similar to the B19′ structure with a larger monoclinic angle. Most notably, the volume is greater due to a large elongation of the *a* lattice constant. This will be discussed later in conjunction with the atomistic transformation path.

We also attempted to calculate a path to the B33 phase, proposed by Refs. 2 and 9, but this caused an impractical 10.1% elongation of the *a* lattice constant when the final structure was reached. While the total energy of this calculated B33 phase is 3 meV/atom lower than B19′, it is improbable that such transformation would occur within a bulk system. Instead, the system is likely to stabilize the B19′ phase with internal stresses (as Huang *et al.* proposed[2]), and the B2→B19′ transformation will follow our calculated path in which no lattice constant is distorted by more than 3%.

Having determined the transformation path of NiTi, we now focus on the electronic origin driving this martensitic process. This behavior was traced to the electronic structure by Zhao *et al.*[20] who discovered nesting of the Fermi surfaces in the [110] direction. Our calculations show that these plane parallel regions [Fig. 4(a)], which correspond to, and are verified by, soft phonon modes in dispersion measurements and calculations,[21–23] lie in the [110] and [111] directions of the B2 structure and give rise to charge-density wave formation, which in turn displays a structural instability of the B2 phase.

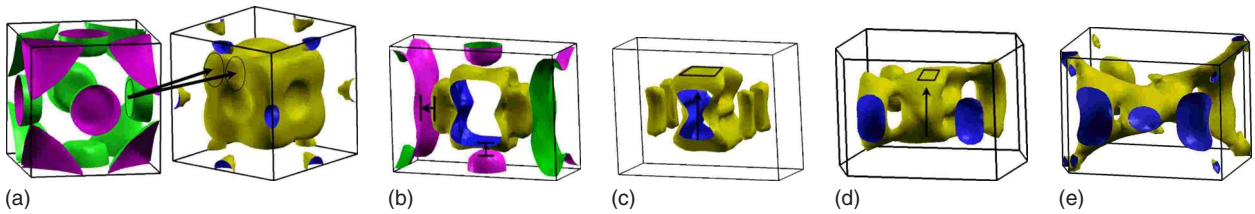

FIG. 4. (Color online) The Fermi surfaces along the transformation path. Arrows represent plane-parallel nested regions. (a) The B2 phase has nesting in [110] and [111]. This agrees with phonon softening experiments (Refs. 21 and 22). (b) At 0.2 ⟨100⟩{011} bilayer shear, there is nesting in the [100] and [001] directions. (c) At 0.5 ⟨100⟩{011} bilayer shear (also 109°-B19′), the nesting has disappeared in the [100] direction and only [001] nesting remains. (d) As the monoclinic angle is relaxed to 103°, the nesting area shrinks to less than a quarter of the original size. (e) Finally, there is no longer any apparent nesting when the monoclinic angle reaches 99°.

Strikingly, as the transformation proceeds from B2, the nesting directions and the soft phonon modes change simultaneously. Nesting in the [110] and [111] directions disappears and appears instead in the [100] and [001] directions [Fig. 4(b)] while the TA_1 phonon mode becomes unstable and is lowered below the others [Fig. 3]. In the ⟨100⟩ direction of the dispersion, TA_1 is completely unstable. This instability, which appears only after B2 begins to transform, drives the transformation via ⟨100⟩{011} bilayer shear and may be traced to the change in Fermi-surface nesting direction. At $0.5u/a$ displacement, the nesting character again changes to intraband and is only present in the [001] direction [Fig. 4(c)]. This drives the second step of the transformation. As the monoclinic angle is relaxed, the nesting area decreases and eventually disappears when the structure becomes B19′ [Figs. 4(d) and 4(e)].

In summary, we have established a unique barrierless mechanism for the NiTi martensitic transformation path, which is enabled by low resistance to ⟨100⟩{011} shear, small C_{44} and C' elastic constants, and instabilities in the electronic structure and phonon spectrum of the B2 structure. Furthermore, we provide a direct connection between the structural evolution between B2 and B19′ and simultaneous changes of its electronic structure. Anomalies in the Fermi surface and the phonon spectrum at each step along the transformation drive NiTi from austenite to martensite. By linking these phenomena, we provide a clear explanation of the martensitic structural behavior and its origin which can be uncovered through *ab initio* calculations. These findings may be applied to the wide class of materials that exhibit martensitic transformations.

This work was supported by the AFOSR (Grant No. FA9550-07-1-0174) and by the ONR (Grant No. N00014-05-C-0241) and by computer time grants at DOD HPC centers NAVO, ARSC, ASC, and MHPCC. We are grateful to L.-H. Ye and S. H. Rhim for fruitful discussions.

[1] K. Otsuka and X. Ren, Mater. Sci. Eng., A **273**, 89 (1999).
[2] X. Huang, G. Ackland, and K. Rabe, Nature Mater. **2**, 307 (2003).
[3] R. F. Hehemann and G. D. Sandrock, Scr. Metall. **5**, 801 (1971).
[4] G. M. Michal and R. Sinclair, Acta Crystallogr., Sec. B: Struct. Crystallogr. Cryst. Chem. **37**, 1803 (1981).
[5] F. E. Wang, S. J. Pickart, and H. A. Alperin, J. Appl. Phys. **43**, 97 (1972).
[6] Y. Kudoh, M. Tokonami, S. Miyazaki, and K. Otsuka, Acta Metall. **33**, 2049 (1985).
[7] M. Sanati, R. C. Albers, and F. J. Pinski, Phys. Rev. B **58**, 13590 (1998).
[8] S. Prokoshkin, A. Korotitskiy, V. Brailovski, S. Turenne, I. Khmelevskaya, and I. Trubitsyna, Acta Mater. **52**, 4479 (2004).
[9] J. R. Morris, Y. Ye, M. Krcmar, and C. L. Fu, in *Advanced Intermetallic-Based Alloys*, edited by J. Wiezorek, C. L. Fu, M. Takeyama, D. Morris, and H. Clemens, MRS Symposia Proceedings No. 980 (Materials Research Society, Warrendale, PA, 2007), p. II06-10.
[10] P. Sittner, P. Lukas, D. Neov, V. Novak, and D. Toebbens, J. Phys. IV **112**, 709 (2003).
[11] T. Hara, T. Ohba, E. Okunishi, and K. Otsuka, Mater. Trans., JIM **38**, 11 (1997).
[12] T. H. Nam, T. Saburi, Y. Nakata, and K. Shimizu, Mater. Trans., JIM **31**, 1050 (1990).
[13] E. Wimmer, H. Krakauer, M. Weinert, and A. J. Freeman, Phys. Rev. B **24**, 864 (1981).
[14] J. P. Perdew, K. Burke, and M. Ernzerhof, Phys. Rev. Lett. **77**, 3865 (1996).
[15] M. Weinert (unpublished).
[16] J. Gachon, M. Notin, and J. Hertz, Thermochim. Acta **48**, 155 (1981).
[17] T. Ohba, T. Taniwaki, H. Miyamoto, K. Otsuka, and K. Kato, Mater. Sci. Eng., A **438-440**, 480 (2006).
[18] X. Huang, C. Bungaro, V. Godlevsky, and K. M. Rabe, Phys. Rev. B **65**, 014108 (2001).
[19] V. Vitek, Cryst. Lattice Defects **5**, 1 (1974).
[20] G.-L. Zhao, T. C. Leung, B. N. Harmon, M. Keil, M. Müllner, and W. Weber, Phys. Rev. B **40**, 7999 (1989).
[21] P. Moine, J. Allain, and B. Renker, J. Phys. F: Met. Phys. **14**, 2517 (1984).
[22] H. Tietze, M. Mullner, and B. Renker, J. Phys. C **17**, L529 (1984).
[23] K. Parlinski and M. Parlinska-Wojtan, Phys. Rev. B **66**, 064307 (2002).
[24] K. Parlinski, Z. Q. Li, and Y. Kawazoe, Phys. Rev. Lett. **78**, 4063 (1997).